Simulation of a Full Fuel Cell Membrane Electrode Assembly Using Pore Network Modeling

Mahmoudreza Aghighi,[a,*] Michael A. Hoeh,[b] Werner Lehnert,[b,c,] Geraldine Merle,[a] and Jeff Gostick[a,**,z]**

[a]*McGill University, Department of Chemical Engineering, Montreal, Quebec H3A 0C5, Canada*
[b]*Forschungszentrum Jülich GmbH, Institute of Energy and Climate Research, IEK-3: Electrochemical Process Engineering, 52425 Jülich, Germany*
[c]*Modeling in Electrochemical Process Engineering, RWTH Aachen University, Aachen, Germany*

A pore network model has been applied to a both sides of a fuel cell membrane electrode assembly. The model includes gas transport in the gas diffusion layers and catalyst layers, proton transport in the catalyst layers and membrane, and percolation of liquid water. This paper presents an iterative algorithm to simulate a steady state isothermal cell with a 3D pore network model for constant voltage boundary condition. The proposed algorithm provides a simple method to couple the results of the anode and the cathode sides by iteratively solving the uncoupled equations of the transport processes. It was found that local water blockages at the GDL/CL interface not only affect concentration polarization, but also might change ohmic polarization of the cell. Depending on the liquid water configuration in the porous electrodes, the protons generated in the anode need to travel longer paths to reach the active sites of the cathode; consequently, the IR loss will be increased in the presence of liquid water. This finding highlights the strength of pore network models which resolve discrete water blockages in the electrodes.

Manuscript submitted November 16, 2015; revised manuscript received January 7, 2016. Published January 29, 2016. This was Paper 1044 presented at the Cancun, Mexico, Meeting of the Society, October 5–9, 2014.

Polymer electrolyte membrane fuel cells are one of the key technologies required to realize a sustainable energy economy because they provide energy storage. A typical PEMFC is a stack of electrochemical cells, and the heart of each is a sandwich of several porous layers around a thin polymer electrolyte membrane, referred to as a membrane-electrode assembly (MEA). In the typical arrangement each side consists of a gas diffusion layer (GDL), and a catalyst layer (CL). The GDL is usually a carbon-fiber based paper and acts as a spacer to allow gaseous reactants to reach regions of the catalyst layer under the flow field ribs, and as a bridge to allow electron access to catalyst sites over the flow field channels. The CL is composed of a mixture of ionomer such as Nafion and carbon-supported platinum catalyst particles, and is adhered to the surface of the membrane as a porous coating around 10–20 μm thick. The ionomer phase in the CL allows protons to reach the catalyst sites, while the carbon particles provide pathways for electrons, and the porosity allows transport of gaseous reactants (oxygen and hydrogen) and product (water). Under some conditions the cathode produces liquid water, which can accumulate in the pore spaces, blocking the access to the reaction sites. Liquid water can also be found on the anode side, for instance if temperature fluctuations occur since the hydrogen is humidified. Understanding the role of liquid water and its impact on fuel cell operation has been a longstanding challenge for the industry.[1–3] Complete water removal from the cell is not an option because the currently used membrane materials must be hydrated to function.

When electrical current is drawn, several sources of voltage loss are incurred due to the inefficiencies of current generation and transport processes. Voltage losses can be broken into three categories: activation polarization η_{act}, ohmic polarization η_{IR}, and concentration polarization η_{conc}. Activation losses arise because of the electrochemical kinetics of the catalyst, such as electron transfer, formation of intermediates, etc. Concentration polarization happens when insufficient reactants reach the electrode catalyst. The inadequate concentration at the reaction sites adversely affects the kinetics of the electrochemical reactions. Ohmic losses are mainly caused by interfacial resistances and the transport of protons through the electrolyte. Reduction in any or all of these polarization sources is the key to building more efficient, powerful and cheaper cells.

One of the challenges to understanding fuel cell operation is that numerous transport processes occur in a MEA simultaneously, and they are coupled in complex ways. The presence of liquid water in the porous electrodes of MEA can alter these transport processes in various ways, thus understanding its effect on the cell performance has been a major goal of fuel cell researches.[2,4,5] Wang et al.[6,7] were one of the earliest to model multiphase transport in the GDL using the volume-averaged approach borrowed from groundwater hydrology and reservoir engineering. The atypical properties of MEA components however, such as high porosity, neutral wettability, anisotropy and thinness make modeling them a challenging task for several reasons. Firstly, the constitutive relationships and transport parameters for these materials are not easily measured, particularly for multiphase transport processes. A huge effort in the past decade has largely addressed this problem[8–10] but important issues still remain. As pointed out recently[11] the exact configuration of liquid water in a thin material like a GDL can have an overriding impact on the gas diffusion, meaning that a unique and unequivocal determination may not even be possible. Secondly, the thinness of the materials actually violates many of the basic assumptions of volume-averaged modeling and percolation theory that are generally accepted for reservoir scale simulations.[12] For instance, the use of volume-averaged models implies the presence a representative elementary volume (REV),[13] which practically speaking means that a transport property measured on an REV-sized sample can be confidently applied to all nodes in the computational domain. Due to their thin nature it's not possible to extract a subsample of a GDL for measurement, and moreover, GDLs are sufficiently heterogeneous that an REV cannot be defined.[14] Finally, and most importantly for the present work, volume-averaged models do not resolve discrete water clusters, but rather treat the presence of water as a fractional value between 0 and 1 indicating the extent to which a given region is partially filled with water. This has implications for fuel cell modeling where local starvation of reactants can have significant performance impacts, as will be demonstrated in this work. It should be pointed out that continuum modeling can be applied at the sub-pore-scale without any of the above limitations, since this does not require volume averaging of the porous microstructure. This approach however, comes at a high computational cost, limiting their application to a hand full of pores, especially for multiphase flow.[15]

Pore network modeling (PNM) is an alternative to the traditional volume-averaged approach that is receiving increased interest as a means to model PEMFCs. In pore network modeling, the media is

*Electrochemical Society Student Member.
**Electrochemical Society Member.
[z]E-mail: jeff.gostick@mcgill.ca

mapped as a set of interconnected pores and throats, transport is modeled similar to a resistor network, and capillary behavior is modeled using percolation theory concepts. PNMs are appealing for two main reasons. Firstly, they do not require constitutive relationships that can be so challenging to measure; instead they need only structural information about pores sizes and connectivity as inputs. Secondly, they track discrete water configurations so allow the study of percolation effects and the local impacts of water blockages. While pore network modeling has been extensively used in the study of porous media of geologic origin,[16–18] it has only recently been applied to model transport properties in fuel cell electrodes.[19–21] Gostick et al.[20] used a cubic pore network model to study multiphase mass transfer and capillary properties of GDL, with the aim of estimating experimentally challenging transport parameters such as relative permeability and effective diffusivity that have only recently been measured.[10,22] Many other pore network models have since been developed to study multiphase transport in PEM fuel cells using various types of networks.[23,24] Recently several groups have modelled fuel cell performance including electrochemical polarization behavior using pore networks,[25,26] but these have been confined to modeling the CL only. The full MEA, including both GDLs, CLs and the membrane, of a PEMFC has so far only been covered by volume-averaging approaches.[1] Despite the disadvantages outlined above, they are widely used due to the availability of commercial packages and the ease of integrating multiple physical processes. Recently, Zenyuk et al.[27] attempted to couple pore network modeling with a continuum simulator. Because they were using two distinct simulation packages, their report focused on the best approach to couple them. They proposed three schemes depending on the applied simulation parameters, and eventually concluded that modeling local effective properties by a pore network model and then feeding the outputs into the continuum model was most suitable. This approach, though innovative, is clearly cumbersome and requires a great deal of care to translate the simulation results between the domains.

In this work, we present a methodology for simulating a full MEA within a single framework based on a pore network model. The GDLs was modelled as discrete pores while the CLs and membrane were modeled as continua. This combined approach was necessary because the pores of the CL and membrane are too small to resolve while also modeling the full width of a single channel and rib. This was a computational limitation rather than a fundamental limitation of the methodology.

The ability to model the impact of discrete water blockages using pore network can provide unique insights into the transport processes occurring in the electrodes. As a case study, the present work included water clusters on the anode and/or cathode side and observed increased ohmic losses due to local starvation of reactants; an effect not easily captured with volume-averaged approaches since complete starvation does not occur due to the way gas diffusion through water saturation regions is modelled.

Model Development

The modeling domain for the PEMFC as considered in this work is depicted in Figure 1. The reactant gases can enter cell from the left/right side at the channel area in the separator plates and diffuse through the void spaces of the GDLs to reach the reactive sites at the CLs. The protons generated at the anode CL are transported through the membrane to the cathode CL where they react with oxygen to produce water. The electrons produced in the anode are transported through the fibers of the GDLs to the rib of the separator plates, through the external load, and then to the cathode.

In the MEA model presented here, the channel and rib areas of the flow field plate are included as boundary conditions to the gas diffusion and electron conduction problems, respectively. The two GDLs are modeled as cubic pore networks representative Toray TGP-H-120 as outlined in previous work.[20] The two CLs and the membrane are included in the domain and are directly modeled within the pore network framework, however, they are treated as continua. The continua simplification was necessary due to the vast scale difference between

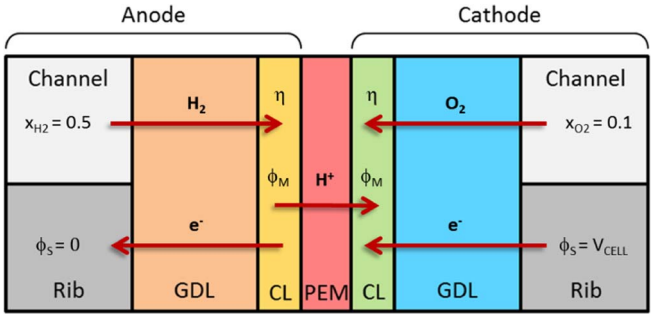

Figure 1. Modeling domain with indication of the variables corresponding to each section. ϕ_M is the membrane (ionomer) phase potential, ϕ_S is the solid (carbon) phase potential, and η is the overvoltage.

the GDL and CL pore sizes. The pores in the GDL are nearly 200 times larger than the CL pores and the extremely small so-called 'pores' of the membrane are only a medium composed of phase segregated regions of the polymer chains.[28] Therefore, instead of explicitly dealing with the massive number of pores in the simulation, the catalyst layer and the membrane are treated as sets of nodes that each represents a segment of the layers as a volume-averaged continua. This approach has been used previously to simulate gas diffusion through the GDL-MPL.[29] Treating the CL as a continua is analogous to the approach of Zenyuk et al.[27] who also treated the CL as a continua and the GDL as a pore network. The key difference is that in the present work the two domains are modelled within the same numerical framework.

Adapting our existing PNM framework (OpenPNM) to solve transport in a continua was possible because pore network models are essentially resistor-networks, so the transport equations are solved using simple finite-difference equations. When treating GDLs as an explicit pore network, the resistor values are dictated by the geometry of the pores and throats (e.g. the hydraulic resistance is found from the Hagan-Poiseuille equation for flow in a tube). In the CLs and membrane, however, the resistor values are determined from the appropriate continuum description of transport (e.g. Darcy's law is applied to each node by assigning a permeability coefficient along with the dimensions of the node). The finite difference method is applied to these continuum nodes so that they can be directly included within the pore network modeling paradigm, despite the fact that finite element approaches are a more powerful and accurate means of modeling continua. Combining the equations into a single, coherent framework was worth any sacrifice in the solution accuracy that may be incurred; especially when considering that any simulation is only as accurate as the available transport parameters and physical constants, which are generally poorly known or even guessed for complex systems such as fuel cells.

Network generation.— The individual networks for the GDLs, CLs and membrane domains are stitched together to form a single modeling domain. The stitching occurs in such a way that the pores on the adjacent interfaces between the networks are connected via throats that span across the interface. In the case of adjacent layers with different spacing (i.e. the GDL-CL interface) each larger pore is connected to multiple nodes on the neighboring domain. This is illustrated in Figure 2. This yields explicitly interconnected domains, avoiding the need for complex coupling techniques using mortars.[30]

In this study, each side of the MEA domain includes a GDL network with a lateral (in-plane) size of 10×10 pores with are spaced $40\ \mu m$ apart. Half of the domain is masked by the flow field rib, meaning that the present model only spans half of a unit cell (half of 1 channel and 1 rib). The GDL was 8 pores thick or $320\ \mu m$. The catalyst domain was $50 \times 50 \times 1$ nodes with $8\ \mu m$ spacing. The CL was treated as a single layer of nodes, but it had physical depth since each node was $8\ \mu m$ deep, so transport resistance into the CL was included. The proposed numerical scheme is fully applicable to CLs with more

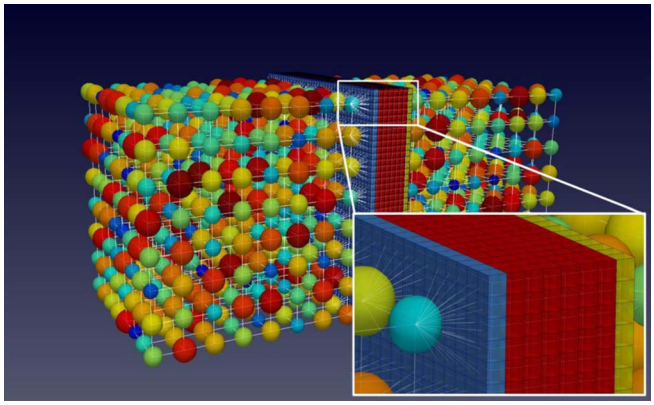

Figure 2. Illustration of interconnections between the GDL domain and the neighboring CL domain. The lattice spacing in the GDL was 40 μm while the spacing of the CL nodes was 8 μm. As can be seen this results in each GDL pore (spheres) connecting to 25 CL nodes (blue cubes).

layers of nodes, but the simple case of 1 layer was sufficient for the present aim of demonstrating the numerical scheme and the benefits of PNMs. The MEA also consists of the membrane layer with a size of $50 \times 50 \times 6$ nodes, also with 8 μm spacing. Thus, to simulate the full MEA, the total unknown variables for each modelled physical process is 21600 in each iteration; however, using the OpenPNM package it is possible to run each algorithm only for the desired subdomain, so that proton transport in the GDL was ignored for instance. This feature of the package significantly facilitates simulation and speeds up the solution procedure.

Model equations.—Usually fuel cells operate at temperature just below 100°C to balance maximizing the intrinsic kinetics while avoiding excessive evaporation of water and drying of the membrane. In this model, operating conditions of 353 (K) and 101325 (pa) are set for the system. It is also assumed that the cell is isothermal, and fully humidified so there will be no water vapor gradient inside the MEA. Consequently, the mass transfer simulation becomes binary diffusion of O_2 (cathode) or H_2 (anode) through a stagnant film of N_2 and/or H_2O (vapor).

Transport in the GDL.—The transport in the GDLs is modeled using established pore-scale physics.[20] Diffusion of A through stagnant B, based on Fick's law using the finite difference scheme, can be obtained by:

$$n_i = \sum_{j=1}^{n} g_{d,ij}(\ln(x_{B,j}) - ln(x_{B,i})) \quad [1]$$

with g_d given by:

$$g_d = \frac{cD_{AB}(2r)^2}{L} \quad [2]$$

where n_i is the mass transfer rate through the throat between pore i and pore j, $x_{B,j}$ is the mole fractions of the stagnant species B in the neighboring pore j, and $x_{B,i}$ is the mole fractions of B in pore i, and g_d is the diffusive conductance of the conduit. In this equation, c is the molar concentration, D_{AB} the binary diffusion coefficient, $2r$ is the width of the conduit and L is the conduit length. The total diffusive conductance for diffusion between two adjacent pore bodies is taken as the net conductance for diffusion through half of body i, the connecting throat and half of body j. The g_d for each section is calculated and the total conductance for the pore-throat-pore assembly is found by:

$$\frac{1}{g_{d,ij}} = \frac{1}{g_{d,bj}} + \frac{1}{g_{d,t}} + \frac{1}{g_{d,bj}} \quad [3]$$

Applying the Equations 1, 2 and 3 for each pore in the network yields a system of linear equations that can be solved with the applied boundary condition on each side of the network to give the concentration distribution across the network.

Transport in the CL.—The effective diffusivity for each node in the CL region is treated as a porous block with a fixed porosity of 0.50 using the following:

$$D_{eff} = D_{bulk}\frac{\epsilon}{\tau}, \quad \tau = (\epsilon)^{-0.5} \quad [4]$$

where ϵ is the porosity and τ is the tortuosity calculated using the Bruggeman relation[31] which is considered to be valid for the granular porous structure of standard CLs. So, the effective diffusive conductance between two nodes in the CL is:

$$g_{d,CL} = \frac{c\, D_{AB}^{eff}\, A}{L} \quad [5]$$

where L and A are length and area of each porous block are set by the node spacing. The same analogy can be applied to ion transport in the ionomer phase (both in the CL and membrane) inside the MEA:

$$g_p = \frac{\sigma_p^{eff}\, A}{L} \quad [6]$$

where g_p is the ionic conductance between the neighboring nodes, which is a function of the node spacing and intrinsic conductivity of the ionomer. The following relation for the effective proton conductivity σ_p^{eff} are used:

$$\sigma_p^{eff} = \sigma_p^{bulk}(\phi_p)^{1.5} \quad [7]$$

where ϕ_p is the ionomer volume fraction and σ_p^{bulk} is the conductivity of the ionomer. The preceding two equations could be used to get the electronic conductivity of the CL, but in the present work the voltage loss due to electron transport was neglected due the extremely high conductivity of the carbon phase.

The transport properties along the throats bridging the CLs and the other subdomains have to be carefully chosen. At the CL-membrane interface, the protonic resistance was the sum of half of a CL node and half of a membrane node, which is the typical pore-network formulation for a conductance between nodes. For the GDL-CL interface throats, however, the resistance of the GDL pore was neglected which assumes that the GDL pore is well mixed, thus diffusion into the CL was only hindered by the resistance of half of a CL node.

Electrochemistry.—The kinetics in the fuel cell and therefore the electron rate was modeled using the following form of Butler-Volmer equations for the anode and cathode reactions at the CLs:[32]

$$J_a = j_0^a\, A_v \left(\frac{C_{H_2}}{C_{H_2}^*}\right)\left[\exp\left(-\frac{\alpha \cdot z_{H2} \cdot F}{RT}\cdot \eta_a\right) - \exp\left(\frac{(1-\alpha)\cdot z_{H_2}\cdot F}{RT}\cdot \eta_a\right)\right] = k_a x_{H_2} \quad [8]$$

and

$$J_c = j_0^c\, A_v \left(\frac{C_{O_2}}{C_{O_2}^*}\right)\left[\exp\left(\frac{\alpha \cdot z_{O_2} \cdot F}{RT}\cdot \eta_c\right) - \exp\left(-\frac{(1-\alpha)\cdot z_{O_2}\cdot F}{RT}\cdot \eta_c\right)\right] = k_c x_{O_2} \quad [9]$$

where α is the transfer coefficient describing the symmetry of the reaction, z_{H_2} and z_{O_2} are the number of electrons involved in the anode and cathode reactions, j_0 is exchange current density, C^* is the reference concentration chosen based on partial pressure of each gas, A_v is the catalyst reactive surface area per unit volume, F is the Faraday constant, $\eta_{a/c}$ describes the activation overvoltage of the anode/cathode reactions, R is the ideal gas constant, T the temperature and J is the

Table I. Summary of the main parameters and properties used in the simulation.

Parameter	Value
Temperature	353 K
Total gas pressure	101325 pa
Open circuit voltage	1.20 V
Diffusivity of O_2 through stagnant cathode film	$2.09 \cdot 10^{-5}\ m^2/s$
Diffusivity of H_2 through stagnant anode film	$1.18 \cdot 10^{-4}\ m^2/s$
Exchange current density (anode)	$1.0 \cdot 10^{-3}\ A/cm^2_{pt}$ [40]
Transfer coefficient (anode)	0.5
Gas relative humidity (anode)	100%
Exchange current density cathode	$1.0 \cdot 10^{-9}\ A/cm^2_{pt}$ [40]
Transfer coefficient (cathode)	0.5
Gas relative humidity (cathode)	100%
Conductivity of MEM	3.0 S/m [41]
Conductivity GDL (Toray TGP-H-120)	1250 S/m [42]
Conductivity of CL	400 S/m [43]
Platinum loading	0.4 mg/cm^2_{cat}
Electrochemical area of Platinum	$6.0 \cdot 10^5\ cm^2_{pt}/g$ [40]
GDL thickness	320 μm
CL thickness	8 μm
Membrane thickness	48 μm
Rib/Channel ratio	0.5
Volume fraction of ionomer in CL	0.3
CL porosity	0.5

current production/consumption rate (A/m^3_{cat}). These kinetic parameters are usually determined from experiments;[33–35] however, since they are highly dependent on temperature, pressure, catalyst-specific parameters and CL structure, wide variations can be found in the literature. Therefore, careful consideration of operational and simulation parameters is required before applying these kinetic values. The values used here are given in Table I.

Water configurations.—An invasion percolation of liquid water algorithm[23,36] is considered by simulating a drainage process of the water into porous electrodes, based on the Washburn equation:

$$P_{c,i} = -2\sigma \frac{cos\theta}{r_i} \quad [10]$$

which $P_{c,i}$ is the capillary entry pressure of pore i with radius r_i, θ is the contact angle of water with the carbon phase, and σ is the surface tension of water. Invasion percolation (IP) algorithm[37] can be used to simulate injection of a fluid into a porous medium in a pore-by-pore fashion. In IP, the invading fluid flows through the accessible throat with the lowest breakthrough capillary pressure. The algorithm starts by finding the accessible throats (i.e. connected to filled pores), then by invading the throat with the lowest entry pressure and simultaneously the other pore connected to that throat. The algorithm continues by adding the throats connected to the newly invaded pore to the list of accessible throats, and so on. Once breakthrough of water into the flow channel occurs, the invasion is halted and this water configuration is considered stable for the remainder of the simulations which assume steady-state conditions.[38]

Iterative algorithm.—A major part of this work was the development of an algorithm able to solve the coupled transport equations for the physics occurring at anode and cathode side. The nature of the PNM framework dictates that each transport process is solved independently, and the coupling occurs through an iterative scheme where results from one solution are used as boundary conditions for another. This iteration procedure is outlined in detail here. Applied boundary conditions required for simulation of an operating MEA are as follows:

- Constant mole fraction of H_2 and O_2 at the GDL/flow channels interface
- Zero mass rate of H_2 and O_2 at the membrane/CL interface
- Zero rate of protons at the CL/GDL interface
- Constant voltage boundary conditions for the solid matrix

The iterative algorithm for this simulation as depicted in Figure 3 is as follows: Two values for η_a and η_c are guessed. An initial guess for these values is obtained by solving a 1D simplified system with spatially averaged properties of the actual network. Starting with an accurate guess drastically reduced the number of iterations required, especially near open-circuit conditions. In subsequent iterations the results of the last step are used and provide an excellent estimation.

Once η_a and η_c are known, the reaction constants k_a and k_c can be found for Eqs. 8 and 9. Based on Faraday's Law of Electrolysis the source/sink terms in the unit volume of catalyst layer will be:

$$S_a = \frac{k_a}{z_{H_2} F} x_{H_2} \quad [11]$$

and

$$S_c = \frac{k_c}{z_{O_2} F} x_{O_2} \quad [12]$$

Then using the overvoltage values and Equations 1, 11 and 12, the rates of hydrogen and oxygen diffusion are computed through the anode/cathode from the flow channels to the catalyst layer. The mass diffusion in both anode and cathode are computed independently. Once the mole fractions are found, the local current per unit volume is determined from the computed local concentration and the kinetic constants based on the current guesses of η_a and η_c in Eqs. 8 and 9:

$$I^a_{local} = k_a\ x_{H_2} \quad [13]$$

and

$$I^c_{local} = k_c\ x_{O_2} \quad [14]$$

By applying the local currents as boundary conditions to the solid phase electron conduction, voltage gradient from the separator plates to the reactive sites can be found. From this step, the solid phase potentials $\phi_{s,a}$ and $\phi_{s,c}$ are obtained, which then permits the computation of the ionomer potentials ($\phi_{m,a}$ and $\phi_{m,c}$) using the definition of overvoltage:

$$\eta_a = \phi_{s,a} - \phi_{m,a} \quad [15]$$

and

$$\eta_c = \phi_{s,c} - \phi_{m,c} - V_{OC} \quad [16]$$

Due to high conductivity of the carbon phase in the GDL and the CL, the voltage distribution will be nearly identical to the respective boundary conditions at each side. The calculation of electron transport can therefore be safely ignored to reduce the number of steps in the algorithm and sped up the solution. With $\phi_{m,a}$ and $\phi_{m,c}$ values known, the protonic conduction through the CL/MEM can be computed for both sides.

The difficulty of this algorithm lies in trying to couple anode and cathode results. This was accomplished by solving two proton conduction problems independently, and iterating until each gave matching results. For the first one, $\phi_{m,a}$ is used as Dirichlet boundary condition with the Neumann boundary condition of the opposing CL (I^c_{local}); and for the second one, $\phi_{m,c}$ is used as Dirichlet boundary condition with I^a_{local} as the Neumann boundary condition. This is indicated Figure 3 as the two arrows connecting the anode and cathode sections of the algorithm. If the solution is converged, then the values of $\phi_{m,a}$ and $\phi_{m,c}$ determined by these two separate algorithms should match the values used as the Dirichlet boundary conditions. The actual convergence check was to compare local current generated in each pore (I^c_{local} and I^a_{local}) to the previous iteration, which was found to be more reliable. The obtained values of $\phi_{m,a}$ and $\phi_{m,c}$ are used to find new values for η_a and η_c from the definitions of overvoltage given above. Direct substitution of η_a and η_c was not stable, so to update the overvoltage guesses it is recommended to use suitable damping factors. In this study, it was found that the damping factor for the overvoltage

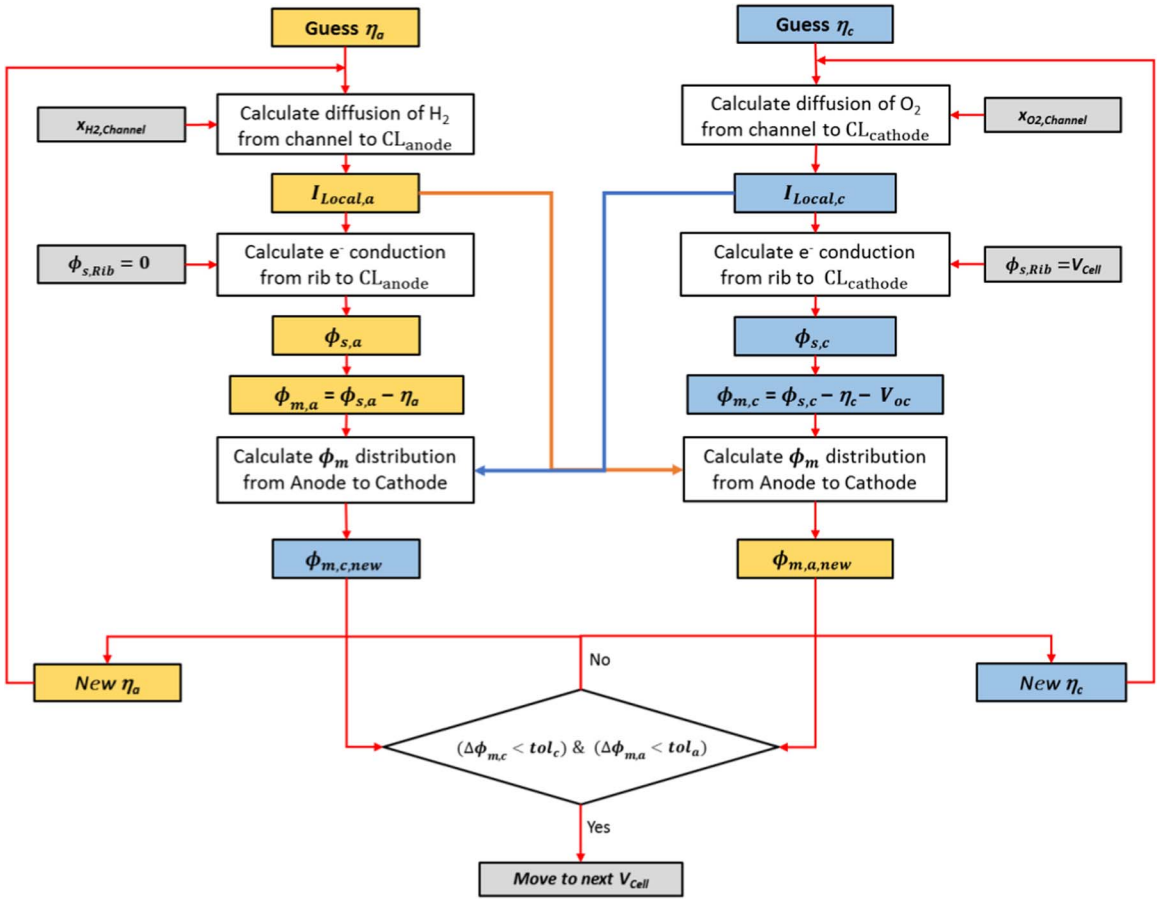

Figure 3. Algorithm diagram of the iterative computational procedure, starting with initial guesses for η_a and η_c , and ultimately obtaining $\phi_{m,a}$, $\phi_{m,c}$ and I_{total}.

guesses should get smaller when lowering the cell voltage. This is numerically beneficial for getting a fast, stable convergence, especially for the concentration polarization dominated region.

The total current produced in the cell can be obtained by:

$$I^a_{total} = \sum_{j=1}^{N} I^a_{local,j} \quad [17]$$

and

$$I^c_{total} = \sum_{j=1}^{N} I^c_{local,j} \quad [18]$$

After numerical convergence has been achieved, it can be confirmed that $I^a_{total} = I^c_{total}$. All of the simulations for this paper have been done by an open source pore network modeling framework named OpenPNM.[39] Also, the main parameters and the properties are summarized in Table I.

Results and Discussion

The iterative algorithm described in the previous section was applied to demonstrate the ability of pore network modeling to simulate a full MEA. The present model did not account for liquid water formation as a result of the thermal conditions in the cell. Instead it was assumed that liquid water was present in 10% of the GDL pores at the GDL-CL interface, then invasion percolation occurred into the GDL from these starting pores until breakthrough was achieved, as outlined in Water configurations section. After placement of the water, simulations of overall cell polarization were conducted. Several cases were considered: A fully humidified cell with no liquid water in the GDL was simulated to provide baseline performance, then liquid water was added to the anode GDL, the cathode GDL or both GDLs (via invasion percolation) to investigate its impact. In addition, sub-cases were compared with fully hydrophobic catalyst layers which were always free of water regardless of water configuration in the adjacent GDL, and partially wettable catalyst layers where a catalyst layer node was filled with water if it was connected to a water-filled GDL pore. This is referred to as 'partially wettable' instead of hydrophilic since the latter unrealistically implies that the CL would become entirely flooded by wicking in water from the GDL. The 'partially wettable' case is meant to capture impact of localized water flooding in the CL.

Hydrophobic CLs.—It was found the hydrophobicity of the CL plays a key role for the cell performance and polarization modeling. Figure 4a shows the polarization curves for the 4 cases with a hydrophobic catalyst layer. Not surprisingly the limiting current is controlled by the conditions on the cathode. The dry cell and the wet anode have nearly identical behavior since the presence of water in the anode GDL does not appreciably hinder the hydrogen diffusion, which has a much higher concentration and higher diffusion coefficient than oxygen on the cathode. When water is present in the cathode the limiting current is reduced by 30%, which seem rather substantial given that the GDL saturation was only 21.6%, but actually agrees with the Bruggeman approximation if air saturation $(1 - s_w)$ is used as a proxy for porosity.

Figure 4b shows the IR portion of the polarization curves for the same 4 cases. The IR contribution to the polarization behavior was calculated using the following equation:

$$V_{IR-loss} = \left| \frac{\sum_t^{N_t} q_t \left(V_{p,i} - V_{p,j}\right)}{I_{total}} \right| \quad [19]$$

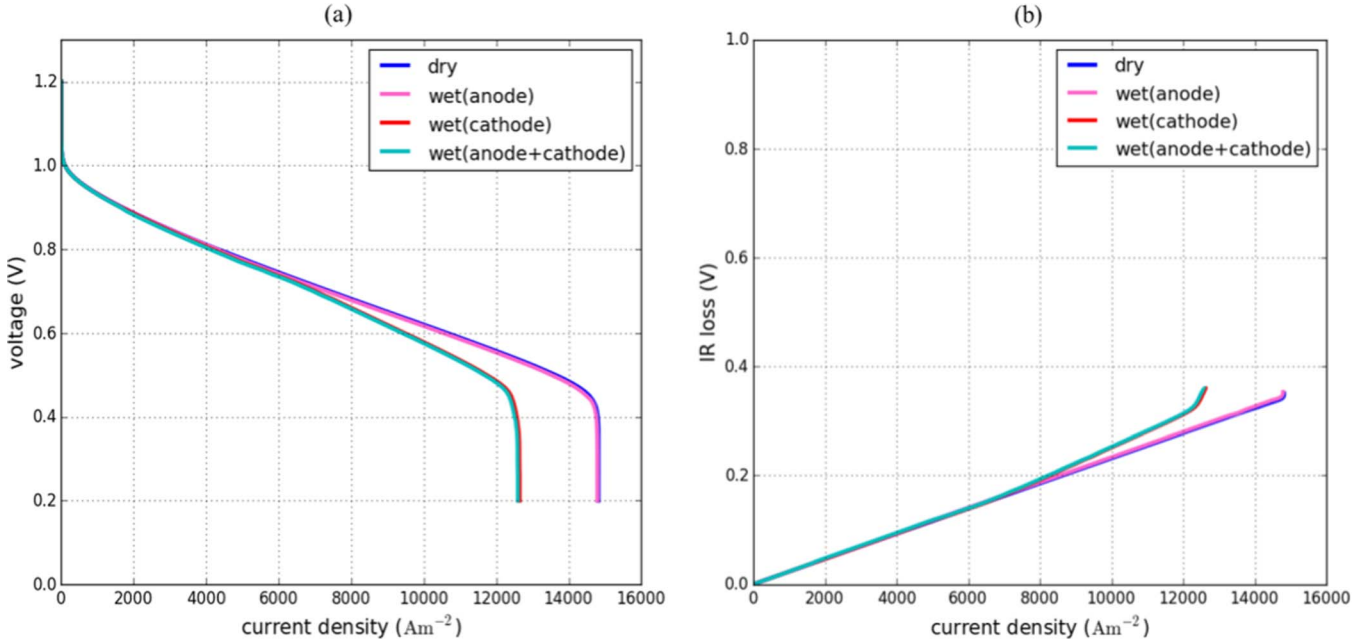

Figure 4. Simulation results for the case of hydrophobic CLs. (a) polarization curve (b) ohmic voltage loss.

where N_t is the total number of the conduits in the membrane and CLs, q_t is the electrical rate between the pores i and j and V_p is the node voltage. As can be seen in Figure 4b, the IR losses for all 4 cases are identical for currents below 700 mA/cm^2, but then diverge. The cases with water on the cathode show an enhanced IR loss above this current which corresponds to the onset of mass transfer limitations. This occurs because regions of the CL located behind water clusters in the GDL become starved for oxygen, and thus are no longer able to consume protons. Consequently, any protons produced on the anode adjacent to these starved regions cannot simply travel across the membrane to a reactive site; instead they must travel laterally to a region of the cathode CL that still has access to oxygen. This effect is illustrated in Figure 5 which is a map of reactant concentrations in the CLs at 0.4 V. There are clearly observed regions in the cathode CL that are completely starved of oxygen (blue) and therefore consuming no protons. In the anode CL hydrogen is distributed uniformly across the CL so proton generated is occurring uniformly across the entire CL. Thus, some of the protons produced in the anode CL must travel farther to reach a reactive region in the cathode CL, indicated by the green arrows, which incurs higher ohmic losses. The presence of water on the anode does not impact this behavior since hydrogen is easily able to diffuse behind the water clusters in the anode CL and achieve a fairly uniform distribution. The hydrogen concentration in the anode was confirmed to be virtually uniform under all conditions.

Partially wettable CLs.—The fully hydrophobic catalyst layer considered in the previous section is probably unrealistic and some liquid water is expected in the CL. In the present work, this scenario was modeled by considering that all CL pores connected to a water filled GDL pore were also water filled. This heuristic approach to water placement is meant only as a means of investigating the impact of water flooding on the CL, and future work will aim to include the behavior of water in the CL. In any event, the approach taken here will at least represent the fact that regions with good reactant access (i.e. away from water clusters) will also be hotter and less likely to contain condensed water.

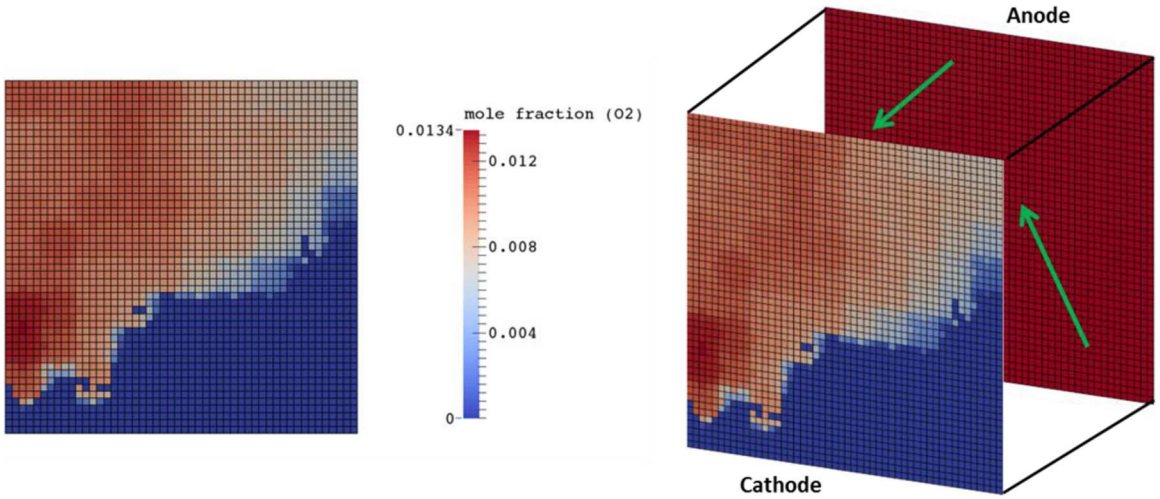

Figure 5. The distribution of oxygen in the cathode catalyst layer (left) at 0.4 V shows regions of oxygen starvation (blue) where no reaction occurs. Some of the protons generated uniformly through the anode must travel longer distances (green arrows) to reach active sites in the cathode.

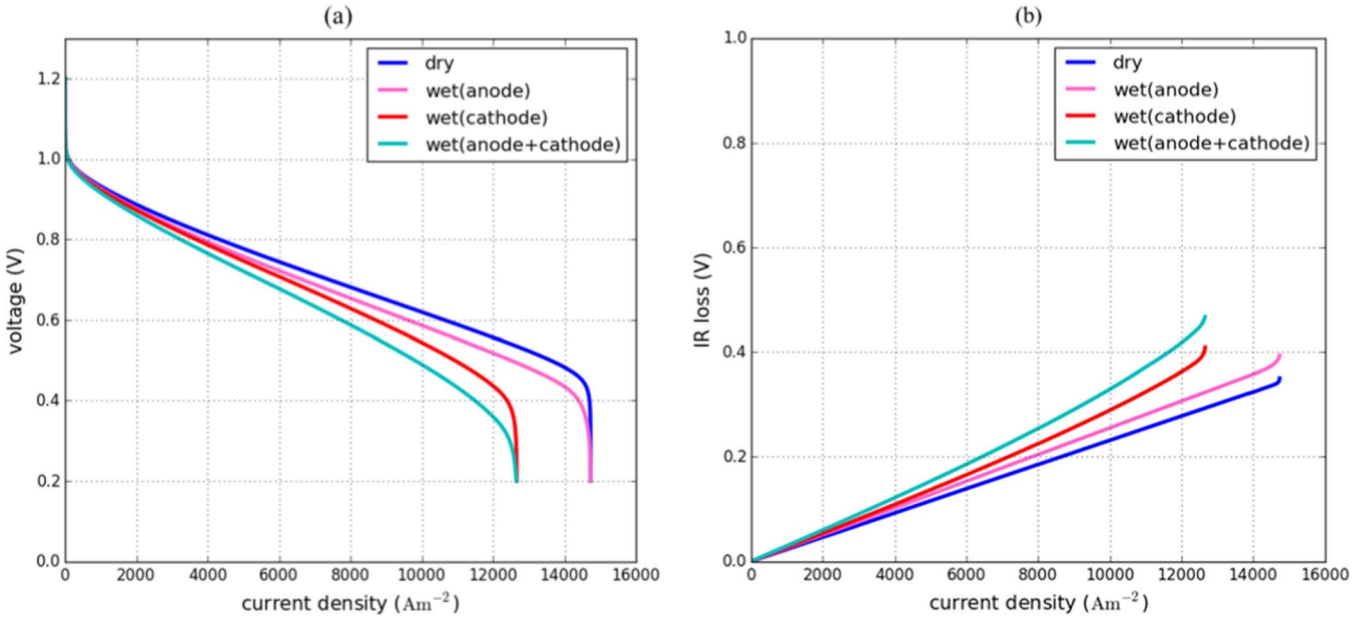

Figure 6. Simulation results for the case of partially wettable CLs. (a) polarization curve (b) ohmic voltage loss.

Figure 6 shows the polarization behavior for the 4 cases (dry, wet anode, wet cathode, and wet anode + cathode) with a partially wettable CL. The water configuration in the GDL for these cases is exactly the same as for the hydrophobic CL cases, so that these results can be compared side-by-side. There are two key features to note. Firstly, the limiting currents for all cases are identical to the hydrophobic CL cases. This is because the total flux of oxygen to the CL is limited by transport through the cathode GDL, which has the same configuration in both cases. Secondly, the IR losses are much higher than the hydrophobic CL cases. It was shown in Hydrophobic CLs section that inactive regions in the cathode CL forced protons produced uniformly across the anode CL to travel longer paths. The presence of water in the anode GDL did not alter this behavior because the high concentration and diffusion coefficient of hydrogen gas allow it to diffuse laterally in the anode CL to maintain a uniform concentration. When water is present inside the anode CL, however, it creates inactive regions since water is essentially impervious to gas transport. Figure 7 shows the gas concentration in both sides of the cell with water-filled pores and nodes removed. The presence of inactive regions in both the anode and cathode CLs caused an additional 20% increase in ohmic losses over a wet cathode alone. This occurs because protons are now produced at a few isolated locations in the anode CL and these are less likely to coincide with an active region in the cathode CL. Figure 8 shows a top-view of each CL colored according to the local ionomer potential, ϕ_m.

The discrete nature of the water blockage in the anode CL impacted the transport processes in important ways. This result was not seen when the anode CL was hydrophobic, since gas could diffuse into the regions behind the water. This highlights the benefit of PNMs over volume-averaged models, since they model local water saturation as a fractional value and effective diffusivity is a continuous function of saturation, which allows gas to diffuse into and through regions that are blocked by water.

Conclusions

In this work, an iterative algorithm was presented that captures a full PEMFC using a multi-domain pore network model to describe

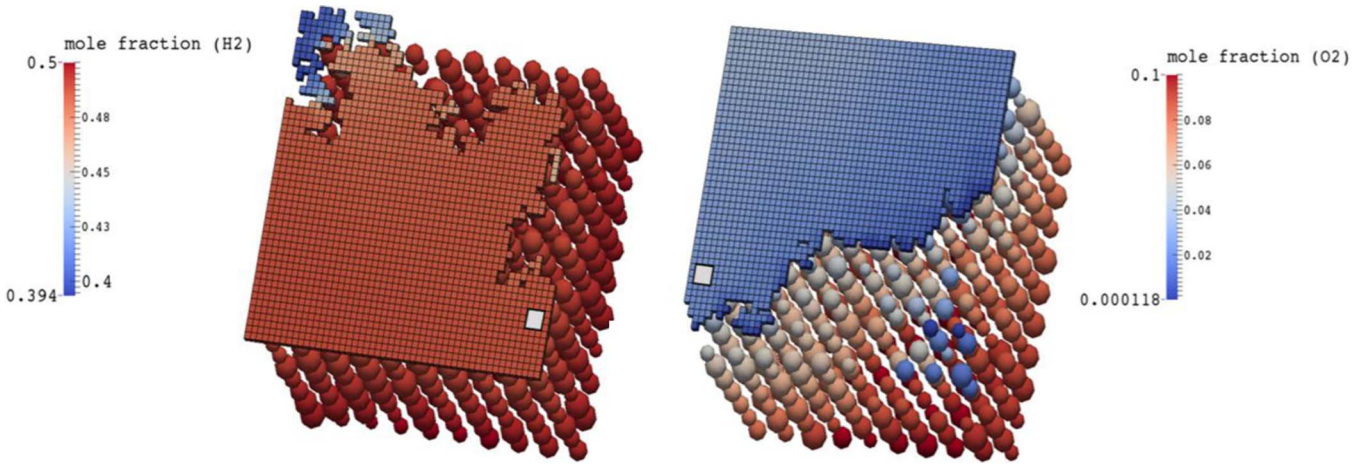

Figure 7. Distribution of reactants for a MEA with wet anode (left) and wet cathode (right) at 0.5 (V). The missing pores and nodes are those blocked due to presence of liquid water. The fiducial marker at each side can be used as a point of reference for connecting the anode and cathode images.

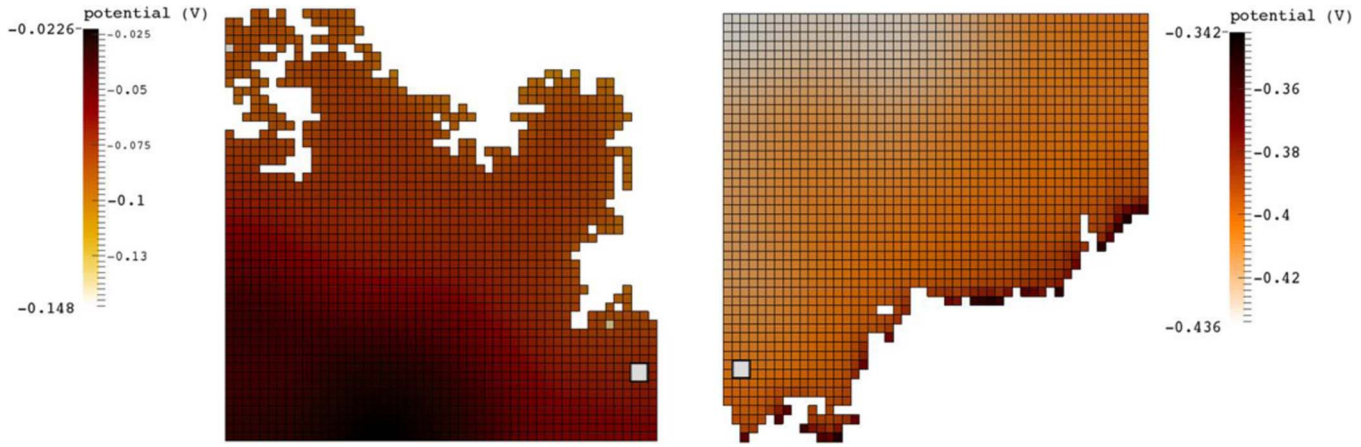

Figure 8. Ionomer potential distribution at the interface between CL and MEM for a MEA with wet anode (left) and wet cathode (right) at 0.5 (V). There is no proton production/consumption in the blocked regions of CL. The fiducial marker at each side can be used as a point of reference for connecting the anode and cathode images.

each part of the membrane electrode assembly. The proposed method applied a constant voltage boundary condition, and couples the transport occurring on the anode and cathode sides of the cell. The gas diffusion layer region was modeled using pore-scale physics, while the catalyst layer was treated as a porous continuum. This approach allowed capturing the blockage of reactive sites on the CLs with water clusters resulting from water percolation in gas diffusion layer. It was shown that the presence of liquid water in the catalyst layer ultimately leads to an increase in ohmic losses and a decrease in cell performance. Being able to capture these effects sets the pore network approach apart from other approaches like volume-averaged modeling, as these effects would be difficult to capture with the volume-averaged approach. The present work was overly simplistic in several regards, such as thermal transport and representing the catalyst layer geometry as a single layer of nodes, but the main focus was on illustrating the numerical scheme. Future work will focus on implementing thermal transport and phase change, calibration of the model against experimental polarization curves, more detailed models for the electrochemical reactions (e.g. carbon corrosion, Pt oxidation), and will increase the resolution of the CL to include several layers thereby allowing through-plane gradients.

Acknowledgments

The authors thank the Natural Science and Engineering Research Council of Canada financial support throughout the course of this project.

References

1. A. Z. Weber, R. L. Borup, R. M. Darling, P. K. Das, T. J. Dursch, W. Gu, D. Harvey, A. Kusoglu, S. Litster, and M. M. Mench, "A Critical Review of Modeling Transport Phenomena in Polymer-Electrolyte Fuel Cells." *Journal of The Electrochemical Society*, **161**(12), F1254 (2014).
2. M. Secanell, J. Wishart, and P. Dobson, "Computational design and optimization of fuel cells and fuel cell systems: a review." *Journal of Power Sources*, **196**(8), 3690 (2011).
3. J. P. Owejan, J. E. Owejan, W. Gu, T. A. Trabold, T. W. Tighe, and M. F. Mathias, "Water transport mechanisms in PEMFC gas diffusion layers." *Journal of The Electrochemical Society*, **157**(10), B1456 (2010).
4. N. Djilali, "Computational modelling of polymer electrolyte membrane (PEM) fuel cells: Challenges and opportunities." *Energy*, **32**(4), 269 (2007).
5. C. Siegel, "Review of computational heat and mass transfer modeling in polymer-electrolyte-membrane (PEM) fuel cells." *Energy*, **33**(9), 1331 (2008).
6. C. Wang, Z. Wang, and Y. Pan, "Two-phase transport in proton exchange membrane fuel cells." *ASME-PUBLICATIONS-HTD*, **364**, 351 (1999).
7. Z. Wang, C. Wang, and K. Chen, "Two-phase flow and transport in the air cathode of proton exchange membrane fuel cells." *Journal of Power Sources*, **94**(1), 40 (2001).
8. J. T. Gostick, M. W. Fowler, M. D. Pritzker, M. A. Ioannidis, and L. M. Behra, "In-plane and through-plane gas permeability of carbon fiber electrode backing layers." *Journal of Power Sources*, **162**(1), 228 (2006).
9. V. Gurau, M. J. Bluemle, E. S. De Castro, Y.-M. Tsou, T. A. Zawodzinski, and J. A. Mann, "Characterization of transport properties in gas diffusion layers for proton exchange membrane fuel cells: 2. Absolute permeability." *Journal of Power Sources*, **165**(2), 793 (2007).
10. I. Hussaini and C. Wang, "Measurement of relative permeability of fuel cell diffusion media." *Journal of Power Sources*, **195**(12), 3830 (2010).
11. P. A. García-Salaberri, G. Hwang, M. Vera, A. Z. Weber, and J. T. Gostick, "Effective diffusivity in partially-saturated carbon-fiber gas diffusion layers: Effect of through-plane saturation distribution." *International Journal of Heat and Mass Transfer*, **86**, 319 (2015).
12. M. Rebai and M. Prat, "Scale effect and two-phase flow in a thin hydrophobic porous layer. Application to water transport in gas diffusion layers of proton exchange membrane fuel cells." *Journal of Power Sources*, **192**(2), 534 (2009).
13. Y. Bachmat and J. Bear, *On the concept and size of a representative elementary volume (REV)*, in *Advances in transport phenomena in porous media.* 1987, Springer. p. 3.
14. P. A. Garcia-Salaberri, J. T. Gostick, G. Hwang, A. Z. Weber, and M. Vera, "Effective diffusivity in partially-saturated carbon-fiber gas diffusion layers: Effect of local saturation and application to macroscopic continuum models." *Journal of Power Sources*, **296**, 440 (2015).
15. A. Q. Raeini, B. Bijeljic, and M. J. Blunt, "Numerical modelling of sub-pore scale events in two-phase flow through porous media." *Transport in porous media*, **101**(2), 191 (2014).
16. I. Chatzis and F. Dullien, "Modelling Pore Structure By 2-D And 3-D Networks With ApplicationTo Sandstones." *Journal of Canadian Petroleum Technology*, **16**(01) (1977).
17. M. A. Celia, P. C. Reeves, and L. A. Ferrand, "Recent advances in pore scale models for multiphase flow in porous media." *Reviews of Geophysics*,**33**(S2), 1049 (1995).
18. M. J. Blunt, "Physically-based network modeling of multiphase flow in intermediate-wet porous media." *Journal of Petroleum Science and Engineering*, **20**(3),. 117 (1998).
19. P. K. Sinha and C.-Y. Wang, "Pore-network modeling of liquid water transport in gas diffusion layer of a polymer electrolyte fuel cell." *Electrochimica Acta*, **52**(28), 7936 (2007).
20. J. T. Gostick,, M. A. Ioannidis, M. W. Fowler, and M. D. Pritzker, "Pore network modeling of fibrous gas diffusion layers for polymer electrolyte membrane fuel cells." *Journal of Power Sources*, **173**(1), 277 (2007).
21. M. El Hannach,, J. Pauchet and M. Prat, "Pore network modeling: Application to multiphase transport inside the cathode catalyst layer of proton exchange membrane fuel cell." *Electrochimica Acta*, **56**(28), 10796 (2011).
22. G. Hwang and A. Weber, "Effective-diffusivity measurement of partially-saturated fuel-cell gas-diffusion layers." *Journal of The Electrochemical Society*, **159**(11), F683 (2012).
23. J. T. Gostick, "Random pore network modeling of fibrous PEMFC gas diffusion media using Voronoi and Delaunay tessellations." *Journal of The Electrochemical Society*, **160**(8), F731 (2013).
24. J. Hinebaugh, Z. Fishman, and A. Bazylak, "Unstructured Pore Network Modeling with Heterogeneous PEMFC GDL Porosity Distributions." *Journal of The Electrochemical Society*, **157**(11), B1651 (2010).
25. M. El Hannach, M. Prat, and J. Pauchet, "Pore network model of the cathode catalyst layer of proton exchange membrane fuel cells: Analysis of water management and electrical performance." *International Journal of Hydrogen Energy*, **37**(24), 18996 (2012).
26. R. Wu, Q. Liao, X. Zhu, and H. Wang, "Pore network modeling of cathode catalyst layer of proton exchange membrane fuel cell." *International Journal of Hydrogen Energy*, **37**(15), 11255 (2012).

27. I. V. Zenyuk, E. Medici, J. Allen, and A. Z. Weber, "Coupling continuum and pore-network models for polymer-electrolyte fuel cells." *International Journal of Hydrogen Energy*.
28. M. Schalenbach, M. A. Hoeh, J. T. Gostick, W. Lueke, and D. Stolten, "Gas Permeation Through Nafion. Part 2: Resistor Network Model." *The Journal of Physical Chemistry C*, 2015.
29. J. T. Gostick, M. A. Ioannidis, M. W. Fowler, and M. D. Pritzker, "On the role of the microporous layer in PEMFC operation." *Electrochemistry Communications*, **11**(3), 576 (2009).
30. M. T. Balhoff, S. G. Thomas, and M. F. Wheeler, "Mortar coupling and upscaling of pore-scale models." *Computational Geosciences*, **12**(1), 15 (2008).
31. D. Bruggeman, "Dielectric constant and conductivity of mixtures of isotropic materials." *Ann Phys (Leipzig)*, **24**, 636 (1935).
32. R. P. O'Hayre, S.-W. Cha, W. Colella, and F. B. Prinz, *Fuel cell fundamentals*. 2006: John Wiley & Sons New York.
33. A. Parthasarathy, S. Srinivasan, A. J. Appleby, and C. R. Martin, "Temperature dependence of the electrode kinetics of oxygen reduction at the platinum/Nafion interface—a microelectrode investigation." *Journal of The Electrochemical Society*, **139**(9), 2530 (1992).
34. K. Neyerlin, W. Gu, J. Jorne, and H. A. Gasteiger, "Determination of catalyst unique parameters for the oxygen reduction reaction in a PEMFC." *Journal of The Electrochemical Society*, **153**(10), A1955 (2006).
35. K. Neyerlin, W. Gu, J. Jorne, and H. A. Gasteiger, "Study of the exchange current density for the hydrogen oxidation and evolution reactions." *Journal of The Electrochemical Society*, **154**(7), B631 (2007).
36. E. W. Washburn, "Note on a method of determining the distribution of pore sizes in a porous material." *Proceedings of the National Academy of Sciences of the United States of America*, 1921: p. 115.
37. D. Wilkinson and J. F. Willemsen, "Invasion percolation: a new form of percolation theory." *Journal of Physics A: Mathematical and General*, **16**(14), 3365 (1983).
38. C. Quesnel, R. Cao, J. Lehr, A.-M. Kietzig, A. Z. Weber, and J. T. Gostick, "Dynamic Percolation and Droplet Growth Behavior in Porous Electrodes of Polymer Electrolyte Fuel Cells." *The Journal of Physical Chemistry C*, **119**(40), 22934 (2015).
39. A. Putz, J. Hinebaugh, M. Aghighi, H. Day, A. Bazylak, and J. T. Gostick, "Introducing OpenPNM: An Open Source Pore Network Modeling Software Package." *ECS Transactions*, **58**(1), 79 (2013).
40. C. A. Reiser, L. Bregoli, T. W. Patterson, S. Y. Jung, J. D. Yang, M. L. Perry, and T. D. Jarvi, "A reverse-current decay mechanism for fuel cells." *Electrochemical and Solid-State Letters*, **8**(6), A273 (2005).
41. A. Parthasarathy, B. Davé, S. Srinivasan, A. J. Appleby, and C. R. Martin, "The platinum microelectrode/Nafion interface: an electrochemical impedance spectroscopic analysis of oxygen reduction kinetics and Nafion characteristics." *Journal of The Electrochemical Society*, **139**(6), 1634 (1992).
42. M. Mathias, J. Roth, J. Fleming, and W. Lehnert, *Diffusion media materials and characterisation*. *Handbook of fuel cells*, 2003.
43. H. Meng and C.-Y. Wang, "Electron transport in PEFCs." *Journal of The Electrochemical Society*, **151**(3), A358 (2004).